magnetochemistry

MDPI

Article

Novel Structures and Magnetic Properties of Two [Mn_2] Complexes with 2,4-di-2-pyridyl-2,4-pentanediol as the Ligand

En-Che Yang [1,*], Yu-Ying Chang [1], Shi-Yi Huang [1], Ling-Xuan Hong [1], Gene-Hsiang Lee [2], Hwo-Shuenn Sheu [3] and Chung-Kai Chang [3]

[1] Department of Chemistry, Fu Jen Catholic University, Hsinchuang, New Taipei 24205, Taiwan
[2] Instrumentation Centre, College of Science, National Taiwan University, Taipei 10672, Taiwan
[3] National Synchrotron Radiation Research Center, NSRRC, Hsinchu 30076, Taiwan
* Correspondence: 071549@mail.fju.edu.tw; Tel.: +11-8862-2905-3571

Received: 15 June 2019; Accepted: 10 July 2019; Published: 13 July 2019

Abstract: Two ligands, 2,4-di-2-pyridyl-2,4-pentanediol (rD and mD), were employed to synthesize two Mn_2 complexes, [Mn_2(rD)$_2$$Br_2$] (**1**) and [$Mn_2(mD)_2$($H_2O$)$_2$]$Br_2$ (**2**). Compound **1** crystallized in a tetragonal space group, $P4_12_12$, with a novel hamburger shaped structure. A detailed study indicated that compound **1** did not contain a metal–metal bond, but antiferromagnetic coupling was observed between the Mn(III) ions. Compound **2** crystallized in a monoclinic space group, C2/c, with one Mn(II) and the other with Mn(IV). The two manganese ions were bridged by two alkoxide ligands, resulting in ferromagnetic coupling. Magnetic property studies confirm the above assignments.

Keywords: Magnetic; Mn_2; Manganese; 2,4-di-2-pyridyl-2,4-pentanediol

1. Introduction

Manganese containing coordination complexes are of great interest due to their unique magnetic properties [1–3] as well as their variety of functions in chemistry [4–6]. A very large number of oxygen bridging compounds have been synthesized [7–24]. However, in a survey of the literature, all of the manganese ions in these complexes are connected with neighboring manganese ions through bridging atoms. The only example of a complex where manganese atoms are in direct contact is the well known $(OC)_5$Mn-Mn$(CO)_5$ complex, which contains a single metal–metal bond between the two Mn units [25]. Because the unpaired electrons on the metal centers are paired, this moiety is therefore diamagnetic. Except for this example, there are no reports in the literature of a capped form of a structure with a direct Mn–Mn bond. Nevertheless, in our attempts to use the 2-(2-pyridyl)-isopropanol (dmhmp-H) ligand to synthesize a manganese cluster, we accidently but repeatedly isolated a small amount of a capped form of an Mn_2 complex. Although only small amounts of a dark-green complex were isolated, elemental analysis as well as an XRD powder pattern indicated that it was a highly pure compound. Due to its special structure, we attempted to develop a method to systematically prepare this compound. Based on the X-ray structure, we concluded that the ligand was a racemate of 2,4-di-2-pyridyl-2,4-pentanediol (rD). Numerous efforts were made to optimize the yield, but they were not successful [26]. In a search of the literature, we found that Shopov and co-workers [27] encountered a situation that was very similar to ours, i.e., the most efficient route for preparing such complexes is to start by preparing dmhmp-H from a Grignard reagent [27,28]. We then used MeMgI as the starting material and purified the product by distillation followed by flash column chromatography. Approximately 1% of the racemate and the meso 2,4-di-2-pyridyl-2,4-pentanediol (rD and mD) were obtained, respectively. Armed with the pure ligands, we were then able to generate isolable amounts

of the capped form of the $[Mn_2(rD)_2Br_2]$ (**1**) complex. For a comparison in magnetic property studies, we also used the same procedure for preparing compound **1** to synthesize $[Mn_2(mD)_2(H_2O)_2]Br_2$ (**2**). The magnetic properties of compound **2** remained unreported, although a similar compound with different counter ions, $[Mn_2(mD)_2(H_2O)_2](NO_3)_2$, was reported by Shopov and co-workers [27]. In this report, we describe the novel structure of compound **1** and the magnetic properties of both compounds **1** and **2**.

2. Results and Discussion

2.1. Description of Structures

The 2,4-di-2-pyridyl-2,4-pentanediol (rD and mD) ligands (see Scheme 1) were crucial for preparing these complexes. With the same synthetic approach, different ligands (rD and mD) led to different structures. Numerous efforts were made to synthesize these ligands, but none were successful. Finally, we realized that the best strategy for producing the products was the original reaction condition used for the synthesis of dmhmpH. The Grignard reagent automatically led to minor but promising amounts of rD and mD. After careful work on distillation and chromatography, a reasonable amount of rD and mD ligands could be obtained.

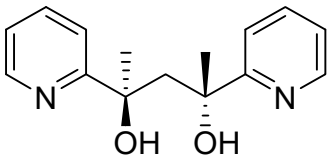

2,4-Pentanediol-2,4-di-2-pyridinyl-(2R,4S)-rel (rD)

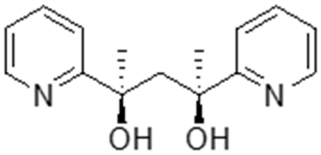

2,4-Pentanediol-2,4-di-2-pyridinyl-(2R,4R)-rel (mD)

Scheme 1. Structural representations of the ligands rD and mD.

Compound **1** crystallized in a tetragonal space group, $P4_12_12$. X-ray refinement data for the complex are listed in Table 1. The structural plot of complex **1** is presented in Figure 1. The structure clearly shows that two manganese ions were penta-coordinated and approached each other through the flat vacancy site of the square-pyramidal structure. Two rD ligands held these two ions in a hamburger form through the nitrogen atoms of the pyridine and the oxygen atom from the alkoxide arm. Two bromide ions functioned as caps from both the top and the bottom of the complex. The metal–ligand bond lengths are shown in Table 2, which shows that the equatorial metal–ligand bond lengths were from 1.846 to 2.003 Å, while the axial Mn–Br bond was 2.5853(7) Å [29,30]. This character clearly indicated a z-out form of the Jahn–Teller distortion of Mn(III) ion. Both the bond valence sum (BVS) calculation (see supporting information) and the charge balance supported our charge assignments. We know that the Mn(III) ions have the same electron configuration as Cr(II), in which the Cr–Cr quadrupole bonds are seen in face-to-face forms of many chromium dimers [31,32]. Nevertheless, the metal–metal distances were maintained at a distance of 3.69 Å from each other, which prevented significant metal–metal bond formation. We therefore became curious about the metal–metal interactions at such a distance. In the discussion below, we conclude that, instead of metal–metal bonds, there was strong antiferromagnetic coupling between these two Mn(III) ions.

Table 1. Refined crystal data and unit cell information.

Empirical Formula	$C_{30}H_{32}N_4O_4Br_2Mn_2$	$C_{30}H_{44}N_4O_{10}Br_2Mn_2$
Fw	782.3	890.39
Space Group	$P4_12_12$	C2/c
a, Å	10.1069(5)	27.9847(12)
b, Å	10.1069(5)	8.3508(3)
c, Å	29.1085(16)	19.8000(8)
α, deg	90	90
β, deg	90	129.3794(10)
γ, deg	90	90
V, (Å^3)	2973.4(3)	3576.6(2)
Z	4	4
ρ(calc), Mg/m^3	1.748	1.654
T, K	150(2)	150(2)
λ, Å	0.71073	0.71073
θ range (deg)	2.133–27.499	2.614–30.000
hkl ranges	−10<=h<=12, −13<=k<=13, −37<=l<=37	−39<=h<=39, −11<=k<=11, −27<=l<=27
Reflections collected	18008	17265
Independent reflections	3411 [R(int) = 0.0354]	5220 [R(int) = 0.0262]
μ, mm^{-1}	3.580	2.999
GOF	1.139	1.052
R_1 [I > 2σ(I)]	0.0224	0.0228
wR_2	0.0547	0.0571
Flack parameter	0.009(5)	

$R_1 = \Sigma||F_0| - |F_c||/\Sigma|F_0|$; $wR_2 = [\Sigma w(F_0^2 - F_c^2)^2/\Sigma w(F_0^2)^2]^{1/2}$; GOF = $\sqrt{\frac{\sum_{hkl} w\Delta^2}{m-n}}$

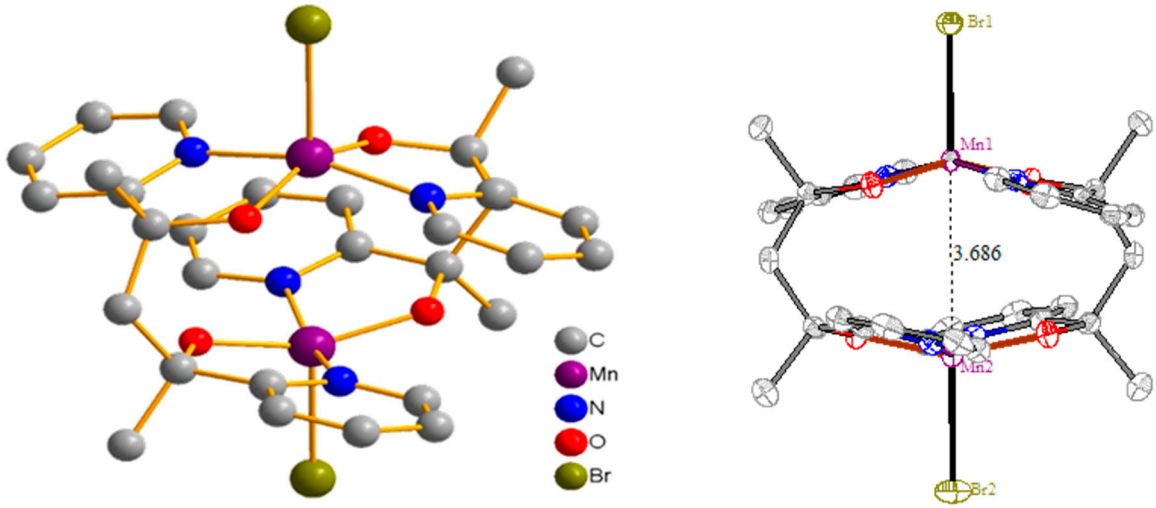

(**a**) (**b**)

Figure 1. (**a**) Structural plot of compound **1**. (**b**) Side view of compound **1**, where the Mn–Mn distance is 3.686 Å.

Compound **2** crystallized in a monoclinic C2/c space group. X-ray refinement data for the complex are also listed in Table 1. The structural plot of complex **2** is displayed in Figure 2. Two manganese ions were held by two double deprotonated ligands with one bound by four alkoxy-groups and two pyridines, the other bound by two bridging alkoxides, two pyridines, and coordinates to two water molecules. Both of the manganese ions were six coordinated, but their charges were quite different. The Mn(1) ion had two metal–ligand bonds with distances of 1.85 Å, two with distances of 1.91 Å, and

bound with pyridine at a distance of 1.99 Å. Since all six metal–ligand bonds were short, we assigned this atom as an Mn(IV) ion. In contrast, Mn(2) bound with a bridging alkoxide at a distance of 2.13 Å, with two water molecules with a distance of 2.18 Å and two pyridines at 2.31 Å. These metal–ligand bonds were obviously long and were therefore assigned as an Mn(II) ion. (See Table 3) This assignment was also supported by bond-valence-sum (BVS) calculations. As described below, we concluded that, as the half filled d orbital in the Mn(II) ion overlapped the empty e_g orbital of the neighbor Mn(IV) ion, this actually triggered the ferromagnetic coupling of compound **2**.

Table 2. Selected bond distances (Å) and angles (deg) of compound **1**.

Mn(1)-O(1)	1.846(2)	Mn(2)-O(2)	1.854(2)
Mn(1)-O(1)#1	1.846(2)	Mn(2)-O(2)#1	1.854(2)
Mn(1)-N(1)	2.003(2)	Mn(2)-N(2)	2.004(2)
Mn(1)-N(1)#1	2.003(2)	Mn(2)-N(2)#1	2.004(2)
Mn(1)-Br(1)	2.5853(7)	Mn(2)-Br(2)	2.5710(7)
O(1)-Mn(1)-O(1)#1	152.66(13)	O(2)-Mn(2)-O(2)#1	155.75(15)
O(1)-Mn(1)-N(1)	82.98(10)	O(2)-Mn(2)-N(2)	82.57(9)
O(1)#1-Mn(1)-N(1)	92.34(10)	O(2)#1-Mn(2)-N(2)	93.92(9)
O(1)-Mn(1)-N(1)#1	92.34(10)	O(2)-Mn(2)-N(2)#1	93.92(9)
O(1)#1-Mn(1)-N(1)#1	82.98(10)	O(2)#1-Mn(2)-N(2)#1	82.58(9)
N(1)-Mn(1)-N(1)#1	160.16(13)	N(2)-Mn(2)-N(2)#1	163.33(16)
O(1)-Mn(1)-Br(1)	103.67(7)	O(2)-Mn(2)-Br(2)	102.12(8)
O(1)#1-Mn(1)-Br(1)	103.67(7)	O(2)#1-Mn(2)-Br(2)	102.12(8)
N(1)-Mn(1)-Br(1)	99.92(6)	N(2)-Mn(2)-Br(2)	98.33(8)
N(1)#1-Mn(1)-Br(1)	99.92(6)	N(2)#1-Mn(2)-Br(2)	98.33(8)

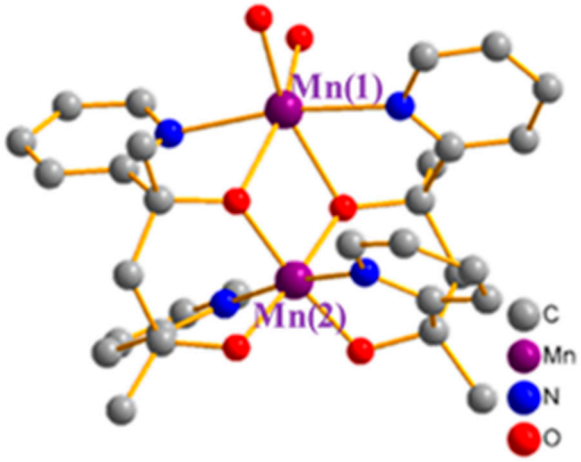

Figure 2. Structural plot of compound **2**. The Mn ion on the top represents Mn(II) and the one on the bottom is Mn(IV).

To further confirm the assignments of the charges for the metal ions, BVS [33] approximations were carried on both compounds **1** and **2**. The calculations were based on Equation (1), where the parameter B was an experience constant with the value 0.37 and the r_0 values were obtained from literature reports and are listed in Table 4. The metal–ligand bond lengths listed in Tables 2 and 3 were then substituted into Equation (1), which indicated that both manganese ions in compound **1** were Mn(III) ions, whereas the metal centers in compound **2** were Mn(II) and Mn(IV) ions [34–37].

$$V = \sum_i S_i = \sum_i \exp\left(\frac{r_0 - r}{B}\right) \quad (1)$$

Table 3. Selected bond distances (Å) and angles (deg) of compound **2**.

Mn(1)-O(3)#1	2.1223(10)	Mn(2)-O(2)#1	1.8435(9)
Mn(1)-O(3)	2.1223(10)	Mn(2)-O(2)	1.8436(9)
Mn(1)-O(1)	2.1832(9)	Mn(2)-O(1)	1.9049(8)
Mn(1)-O(1)#1	2.1832(9)	Mn(2)-O(1)#1	1.9049(8)
Mn(1)-N(1)	2.3073(11)	Mn(2)-N(2)#1	1.9862(11)
Mn(1)-N(1)#1	2.3073(11)	Mn(2)-N(2)	1.9862(11)
O(3)#1-Mn(1)-O(3)	90.13(6)	O(1)-Mn(2)-O(1)#1	85.63(5)
O(3)#1-Mn(1)-O(1)	102.84(4)	O(2)#1-Mn(2)-N(2)#1	80.90(4)
O(3)-Mn(1)-O(1)	156.24(4)	O(2)-Mn(2)-N(2)#1	93.45(4)
O(3)#1-Mn(1)-O(1)#1	156.24(4)	O(1)-Mn(2)-N(2)#1	92.28(4)
O(3)-Mn(1)-O(1)#1	102.84(4)	O(1)#1-Mn(2)-N(2)#1	93.67(4)
O(1)-Mn(1)-O(1)#1	72.74(4)	O(2)#1-Mn(2)-N(2)	93.45(4)
O(3)#1-Mn(1)-N(1)	99.60(4)	O(2)-Mn(2)-N(2)	80.90(4)
O(3)-Mn(1)-N(1)	86.97(4)	O(1)-Mn(2)-N(2)	93.67(4)
O(1)-Mn(1)-N(1)	71.43(4)	O(1)#1-Mn(2)-N(2)	92.28(4)
O(1)#1-Mn(1)-N(1)	100.88(4)	N(2)#1-Mn(2)-N(2)	171.90(6)
O(3)#1-Mn(1)-N(1)#1	86.96(4)	O(2)#1-Mn(2)-Mn(1)	133.89(3)
O(3)-Mn(1)-N(1)#1	99.60(4)	O(2)-Mn(2)-Mn(1)	133.89(3)
O(1)-Mn(1)-N(1)#1	100.87(4)	O(1)-Mn(2)-Mn(1)	42.82(3)
O(1)#1-Mn(1)-N(1)#1	71.43(4)	O(1)#1-Mn(2)-Mn(1)	42.82(3)
N(1)-Mn(1)-N(1)#1	170.75(6)	N(2)#1-Mn(2)-Mn(1)	94.05(3)
O(3)#1-Mn(1)-Mn(2)	134.94(3)	N(2)-Mn(2)-Mn(1)	94.05(3)
O(3)-Mn(1)-Mn(2)	134.94(3)	C(6)-O(1)-Mn(2)	127.13(7)
O(1)-Mn(1)-Mn(2)	36.37(2)	C(6)-O(1)-Mn(1)	115.89(7)
O(1)#1-Mn(1)-Mn(2)	36.37(2)	Mn(2)-O(1)-Mn(1)	100.81(4)
N(1)-Mn(1)-Mn(2)	85.38(3)	C(8)-O(2)-Mn(2)	111.86(7)
N(1)#1-Mn(1)-Mn(2)	85.38(3)	C(5)-N(1)-C(1)	118.48(11)
O(2)#1-Mn(2)-O(2)	92.22(5)	C(5)-N(1)-Mn(1)	114.76(8)
O(2)#1-Mn(2)-O(1)	172.42(4)	C(1)-N(1)-Mn(1)	125.45(9)
O(2)-Mn(2)-O(1)	91.48(4)	C(13)-N(2)-C(9)	121.39(11)
O(2)#1-Mn(2)-O(1)#1	91.48(4)	C(13)-N(2)-Mn(2)	126.02(9)
O(2)-Mn(2)-O(1)#1	172.42(4)	C(9)-N(2)-Mn(2)	112.58(8)

Table 4. r_0's value for Mn with different charges bonds to O, N, and Br atoms.

Mn^{II}-O	Mn^{II}-N	Mn^{II}-Br
1.765	1.849	2.34
Mn^{III}-O	Mn^{III}-N	Mn^{III}-Br
1.732	1.837	2.315
Mn^{IV}-O	Mn^{IV}-N	Mn^{IV}-Br
1.75	1.822	2.41

Powder X-ray Diffraction Patterns: To demonstrate the integrity of the bulk samples of compounds **1** and **2**, series powder X-ray diffraction experiments were performed. Powder X-ray diffraction patterns were collected at the Taiwan Photon Source (TPS) of the National Synchrotron Radiation Research Center (NSRRC). The powder X-ray diffraction pattern of compounds **1** and **2** are shown in Figure 3. The simulated powder patterns of the single crystal data were also plotted together for comparison. The experimental synchrotron radiation X-ray powder diffraction patterns of both compounds **1** and **2** were very close to the single crystal simulation results. This result clearly showed that the bulk samples had good integrity.

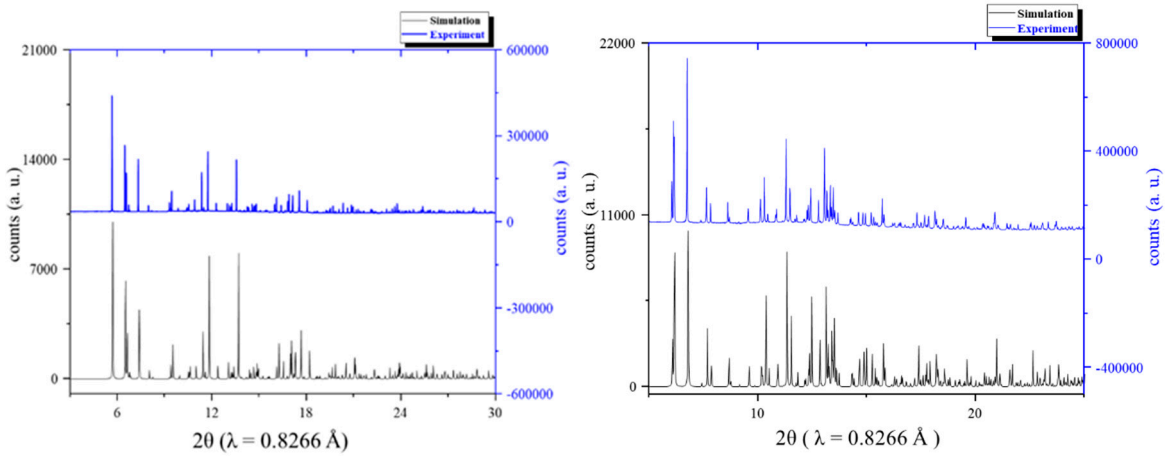

Figure 3. Synchrotron powder X-ray diffraction patterns of experimental data (blue) and simulation (black) for compounds **1** (**left**) and **2** (**right**).

2.2. Magnetic Properties

The magnetic properties of both compounds **1** and **2** could be described as follows: magnetic susceptibility measurements were carried on both compound **1** and compound **2**. Polycrystalline samples restrained in eicosane were measured under a magnetic field of 1000 G in the temperature range 2–300 K. Figure 4 illustrates the $\chi_M T$ vs. T plot of compound **1**. The $\chi_M T$ value was 5.69 $cm^3K\ mol^{-1}$, which was somewhat smaller than the spin only value of 6.0 $cm^3K\ mol^{-1}$ for two uncoupled Mn(III) ions. This could be attributed to antiferromagnetic coupling, even at room temperature. The $\chi_M T$ value slowly decreased to 3.76 $cm^3K\ mol^{-1}$ at 50 K and then decreased very rapidly to 0.17 $cm^3K\ mol^{-1}$ upon further cooling to 2 K. The magnetic behaviors were then interpreted by the Kambe model [38] with:

$$H = g\beta B\cdot(S_1 + S_2) - 2J\ (S_1\cdot S_2) \quad (2)$$

where β is Bohr magneton, B is the magnetic field, and both S_1 and S_2 have the values of 2. The best fitting is presented by the solid red line in Figure 4. The parameters obtained by the fitting gave g = 2.0 and J = −5.0 K, which were in good agreement with the properties of the two Mn(III) ions. Interestingly, the electron configuration of Mn(III) was high spin d^4, which is isoelectronic to Cr(II). By experience, two Cr(II)s in a capped form tend to build up a metal–metal quadrupole bond [39]. However, in our case, it was much more difficult for the Mn(III) to form a metal–metal bond than Cr(II) due to Mn(III) being a harder Lewis acid, whereas the Cr(II) is relatively soft. In addition, in compound **1**, the two Mn(III) ions were separated by a large distance (3.69 Å) by the binding site of ligands. All of these factors reduced the chance to form an actual metal–metal bond, but strong antiferromagnetic couplings were clearly observed.

Figure 5 shows a $\chi_M T$ vs. T plot for compound **2**. The $\chi_M T$ value was 6.39 $cm^3K\ mol^{-1}$, which was slightly higher than the spin only value of 6.25 $cm^3K\ mol^{-1}$ for one uncoupled Mn(IV) and one uncoupled Mn(II). This behavior suggested that ferromagnetic coupling occurred, even at room temperature. The $\chi_M T$ value then increased to 7.98 $cm^3K\ mol^{-1}$ at 15 K and then decreased to 3.58 $cm^3K\ mol^{-1}$ at 2 K. Such behavior is usually attributed to zero-field splitting or intermolecular antiferromagnetic coupling. We then collected magnetic susceptibility data and fitting by utilizing the Kambe model to account for Mn(IV)-Mn(II) above 15 K. The fitting for this appears as a solid red line in Figure 5. The best fitting clearly indicated a ferromagnetic coupling J = +1.8 K, g = 2.0. Judging from the structure, we know there were two unpaired electrons located in the e_g orbitals (d_{x2-y2} and d_{z2}) within the Mn(II) center, whereas these orbitals were empty in the Mn(IV) center. When these two metal ions produced bridging through the x and the y axis, as shown in Scheme 2, the occupied e_g orbitals in Mn(II) right overlapped with the empty e_g orbitals in Mn(IV), which resulted in ferromagnetic coupling between these two ions.

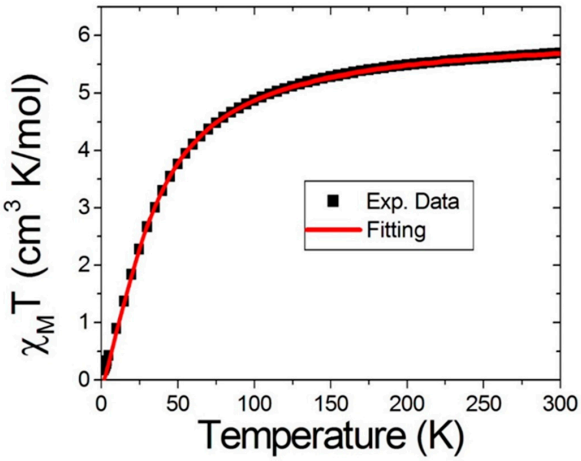

Figure 4. $\chi_M T$ vs. T plot under a magnetic field of 1000 G in the 2~300 K range for compound **1**. The black square represents the experimental data, and the solid red line is the best fit for the data using Equation (2).

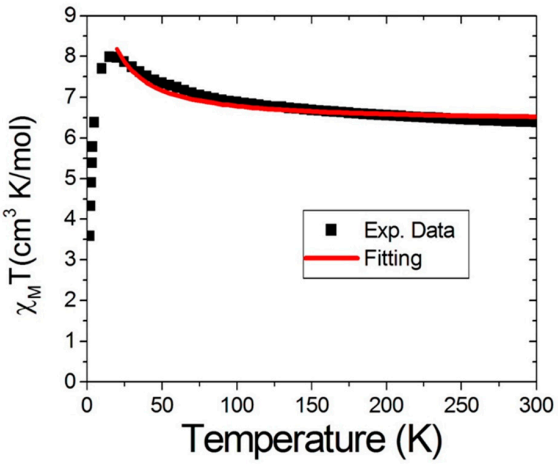

Figure 5. $\chi_M T$ vs. T plot under a magnetic field of 1000 G in the 5~300 K range for compound **2**. The black squares represent experimental data, and the solid red line is the best fit to the data using Equation (1).

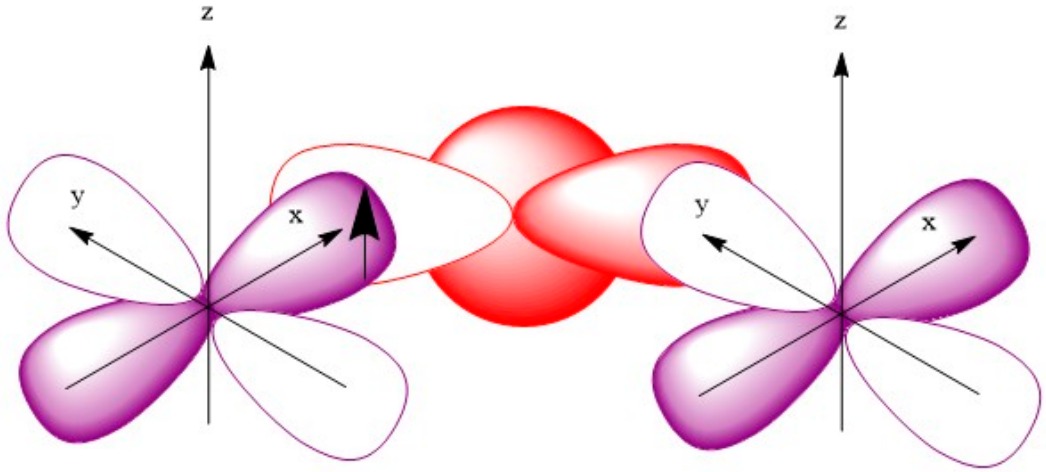

Scheme 2. Orbitals overlap between adjacent Mn(II) and Mn(IV) ions.

To further examine the spin number of the molecule, reduced magnetization measurements were carried on the polycrystalline sample of compound **2** in the temperature range 2~4 K under a magnetic field 2~6 Tesla. The results are shown in Figure 6, where the solid red lines represent the best fitting based on the parameters g = 1.95, S = 4, and D = −0.78 K. The spin value of S = 4 saturated under high-field and low temperatures further confirmed the existence of ferromagnetic coupling between the Mn(II) and Mn(IV) ions.

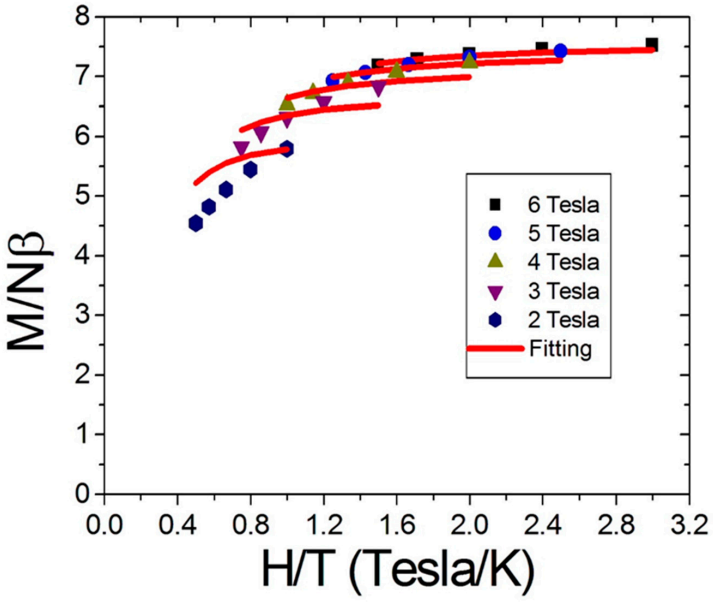

Figure 6. The M/Nβ vs. H/T data indicated that the axial D term for compound **2** was significant.

The alternating current (AC) magnetic susceptibility measurements were also carried out on both compounds **1** and **2** under 1000 Hz of a 3.5 G AC magnetic field in the temperature range 1.9~10 K. Whether a 0 G or a 500 G direct current (DC) magnetic field was applied, no significant out-of-phase signals were detected. This measurement further confirmed that neither **1** nor **2** showed single-molecule magnet (SMM) behavior.

3. Experimental Methods

All chemicals used in this study were of commercial grade and were used without further purification.

3.1. Ligand Synthesis

To a two-neck 250 mL round bottom flask charged with magnesium powder (7.29 g, 300 mmol), 120 mL of anhydrous ethyl-ether was added under a nitrogen atmosphere. Methyl iodide (64 g in 450 mmol) was slowly added over a period of 2~3 h to form the Grignard reagent. Then, 2-Acetylpyridine (18.18 g in 150 mmol) was added to the reactant solution, and the temperature was controlled at –8 °C The reaction was carried out for 5 h and then quenched by adding ice water in an ice bath. Without neutralization, the mixture was extracted by 200 mL ethyl acetate five times. The organic layer was dried over anhydrous $MgSO_4$. After evaporating the organic solvent, the dmhmp-H ligand was removed by distillation under reduced pressure (yield about 70%). The residues were then separated by flash column chromatography eluted with ethyl acetate/hexane (1:1) solution to obtain 1.7% rD, and 1.8% mD was then obtained by eluting pure ethyl acetate.

rD: ^{1}H NMR (300 MHz, $CDCl_3$) δ 1.17 (s, 6H, C***H***$_3$), δ 2.55 (s, 2H HC-***H***), δ 6.24 (br, 2H, O***H***), δ 7.18 (qd, 2H, Py-***H***), δ 7.61 (td, 2H, Py-***H***), δ 7.69 (td, 2H, Py-***H***), δ 8.50 (m, 2H, Py-***H***). ^{13}C NMR $CDCl_3$: δ

166.31, δ 147.34, δ 137.05, δ 121.68, δ 119.44, δ 75.58, δ 50.97, δ 30.56. HRMS (FT-ICR): $[C_{15}H_{18}N_2O_2]H^+$: 259.1441. Found 259.1438.

mD: ^{1}H NMR (300 MHz, $CDCl_3$) δ 1.46 (s, 6H, C***H***$_3$), δ 2.54; 3.02 (d, HC-***H***), δ 6.26 (br, 2H, O***H***), δ 6.78 (qd, 2H, Py-***H***), δ 7.16 (td, 2H, Py-***H***), δ 7.31 (td, 2H, Py-***H***), δ 8.03 (qd, 2H, Py-***H***). ^{13}C NMR $CDCl_3$: δ 164.16, δ 146.66, δ 135.91, δ 120.73, δ 119.89, δ 75.55, δ 50.32, δ 32.68. HRMS (FT-ICR): $[C_{15}H_{18}N_2O_2]H^+$: 259.1441. Found 259.1436.

3.2. Materials Synthesis

$[Mn_2(rD)_2Br_2]$ (1) $MnBr_2{\cdot}4H_2O$ (0.52 g, 1.85 mmol) and ligand rD (0.45 g, 0.88 mmol) were added to 20 mL of acetonitrile. To the mixture, 25% NMe_4OH (0.53 g, 1.46 mmol) was added. The resulting solution was stirred 1~2 h and then passed through a filter. The filtrate was allowed to stand 2~4 days, and dark green crystals suitable for X-ray crystallography analysis were obtained (yield: 80%). Elemental Analysis: ($C_{30}H_{32}N_4O_4Mn_2Br_2$), Found (Calc.):C, 45.87% (46.06%), H, 4.08% (4.12%), N, 7.37% (7.16%). IR (cm^{-1}): 3448 (b), 3079 (s), 2971 (s), 2942 (w), 2921 (w), 1607 (s), 1475 (s), 1181 (s), 1094 (s), 1052 (s), 943 (s), 788 (s), 685 (s), 616 (s), 552 (w), 516 (w).

$[Mn_2(mD)_2(H_2O)_2]Br_2(H_2O)_4$ (2) The same reaction conditions that were used for the preparation of compound (**1**) were used here. $MnBr_2$ $4H_2O$ (0.52 g, 1.85 mmol) and the ligand mD (0.45 g, 0.88 mmol) were added to 20 mL acetonitrile. Then, 25% NMe_4OH (0.53 g, 1.46 mmol) was added to the mixture. The resulting solution was stirred for 1~2 h and then passed through a filter. The filtrate was allowed to stand for 2~4 days, whereupon pink crystals suitable for X-ray crystallographic analysis were formed (yield: 80%). Elemental Analysis: ($C_{30}H_{44}N_4O_{10}Mn_2Br_2$), Found (Calc.):C, 40.12% (40.46%), H, 4.73% (4.98%), N, 6.19% (6.29%). IR (cm^{-1}): 3373 (b), 3068 (b), 1596 (s), 1476 (s), 1435 (s), 1182 (s), 1114 (s), 1097 (s), 1045 (s), 929 (s), 863 (s), 780 (s), 759 (s), 650 (s), 606 (s), 579 (w), 549 (w), 513 (w).

3.3. Physical Property Measurements

NMR spectra were measured on a Bruker AV-300 spectrometer. Infrared spectra were collected using a Perkin Elmer 1600 spectrometer using KBr pellets in the range of 500~4000 cm−^{1}.

DC magnetic susceptibility data were conducted by using a Quantum Design MPMS7 system. Eicosane was employed to restrain the sample to prevent torqueing. The background was corrected by a gel cap charged with eicosane. The diamagnetic correction was estimated by Pascal's constants [40,41].

Elemental analyses were performed by an elemental vario EL cube. All of the measurements regarding magnetic properties and elemental analysis were carried out at the National Taiwan University Instrument Centre, College of Science.

For X-ray crystallography, single-crystal X-ray diffraction data collection was carried out on a Bruker D8 VENTURE CCD diffractometer equipped by Mo, λ = 0.71073 Å as light source. The temperatures were controlled at 150(2) K using an Oxford Cryosystems Cooler. The absorption correction was done by using the SADABS [42] (Bruker 2016) program, which is based on symmetry-equivalent reflections. The structures were solved by direct methods and refined with a full-matrix least-squares technique within the Shelxs-2018 [43] program and refined by the Shelxl-2018 program. [44] All non-hydrogen atoms were refined anisotropically. The hydrogen atoms were set in calculated positions and refined using the riding model. The refinement parameters are summarized in Table 1. CCDC numbers: 1922174 for **1**; 1922175 for **2**.

4. Conclusions

In this paper, we report on the preparation of two 2,4-di-2-pyridyl-2,4-pentanediol (rD and mD) ligands, which were then used to prepare two Mn_2 complexes: $[Mn_2(rD)_2Br_2]$ (1) and $[Mn_2(mD)_2(H_2O)_2]Br_2$ (2). In compound **1**, the rD ligand bound two Mn(III) ions in a hamburger form. Both of the Mn(III) units were five coordinated and approached each other through the flat vacancy site of the square-pyramidal. However, this did not lead to the formation of any metal–metal bond between

these two ions. Upon a magnetic property examination, antiferromagnetic coupling was observed in compound **1**. In compound **2**, the half filled e_g orbitals in Mn(II) were significantly overlapped with the empty e_g orbitals in Mn(IV). This interaction significantly triggered the ferromagnetic coupling of compound **2,** which led to a molecular spin S = 4 and D = −0.78 K. However, this property did not lead to SMM behavior for compound **2**. This manuscript reports not only on a systematic approach for producing both rD and mD ligands but also on their use in forming complexes with novel structures and magnetic properties.

Author Contributions: Conceptualization, E.-C.Y.; Data curation, Y.-Y.C., G.-H.L. and H.-S.S.; Funding acquisition, E.-C.Y.; Investigation, Y.-Y.C., S.-Y.H., L.-X.H., G.-H.L., H.-S.S. and C.-K.C.; Supervision, E.-C.Y.; Writing—original draft, E.-C.Y.

Funding: Ministry of Science and Technology of Taiwan (MOST 106-2113-M-030-008).

Acknowledgments: This work was supported by the Ministry of Science and Technology of Taiwan (MOST 106-2113-M-030-008).

Conflicts of Interest: The authors declare no conflict of interest.

References

1. Christou, G.; Gatteschi, D.; Hendrickson, D.N.; Sessoli, R. Single-Molecule Magnets. *MRS Bull.* **2000**, *25*, 66–71. [CrossRef]
2. Aromi, G.; Aubin, S.M.J.; Bolcar, M.A.; Christou, G.; Eppley, H.J.; Folting, K.; Hendrickson, D.N.; Huffman, J.C.; Squire, R.C.; Tsai, H.L. Manganese Carboxylate Cluster: From Structural Aesthetics to Single-Molecule Magnets. *Polyhedron* **1998**, *17*, 3005–3020. [CrossRef]
3. Christou, G. Single-Molecule Magnets: A Molecular Approach to Nanoscale Magnetic Materials. *Polyhedron* **2005**, *24*, 2065–2075. [CrossRef]
4. Guo, M.; Corona, T.; Ray, K.; Nam, W. Heme and Nonheme High-Valent Iron and Manganese Oxo Cores in Biological and Abiological Oxidation Reactions. *ACS Cent. Sci.* **2019**, *5*, 13–28. [CrossRef] [PubMed]
5. Dismukes, G.C.; Brimblecombe, R.; Felton, G.A.N.; Pryadun, R.S.; Sheats, J.E.; Spiccia, L.; Swiegers, G.F. Development of bioinspired Mn4O4-cubane water oxidation catalysts: Lessons from photosynthesis. *Acc. Chem. Res.* **2009**, *42*, 1935–1943. [CrossRef] [PubMed]
6. Conradie, J.; Tangen, E.; Ghosh, A. Trigonal bipyramidal iron(III) and manganese(III) oxo, sulfido, and selenido complexes. An electronic-structural overview. *J. Inorg. Biochem.* **2006**, *100*, 707–715. [CrossRef]
7. Vinslava, A.; Tasiopoulos, A.J.; Wernsdorfer, W.; Abboud, K.A.; Christou, G. Molecules at the Quantum-Classical Nanoparticle Interface: Giant Mn70 Single-Molecule Magnets of approximately 4 nm Diameter. *Inorg. Chem.* **2016**, *55*, 3419–3430. [CrossRef]
8. Nguyen, T.N.; Shiddiq, M.; Ghosh, T.; Abboud, K.A.; Hill, S.; Christou, G. Covalently Linked Dimer of Mn3 Single-Molecule Magnets and Retention of Its Structure and Quantum Properties in Solution. *J. Am. Chem. Soc.* **2015**, *137*, 7160–7168. [CrossRef]
9. Constantina, P.; Eleni, E.M.; George, C.; Anastasios, J.T. Filling the Gap between the Quantum and Classical Worlds of Nanoscale Magnetism: Giant Molecular Aggregates Based on Paramagnetic 3d Metal Ions. *Chem. Soc. Rev.* **2016**, *45*, 1597–1628.
10. Caneschi, A.; Ferraro, F.; Gatteschi, D.; Melandri, M.C.; Rey, P.; Sessoli, R. Structure and Magnetic Properties of a Dinuclear Manganese(II) Complex with One μ-Aqua and Two μ-Carboxylato Bridges. *Angew. Chem. Int. Ed. Engl.* **1989**, *28*, 1365–1367. [CrossRef]
11. Penner-Hahn, J.E.; Fronko, R.M.; Pecoraro, V.L.; Yocum, C.F.; Betts, S.D.; Bowlby, N.R. Structural characterization of the manganese sites in the photosynthetic oxygen-evolving complex using x-ray absorption spectroscopy. *J. Am. Chem. Soc.* **1990**, *112*, 2549–2557. [CrossRef]
12. Yu, S.B.; Wang, C.P.; Day, E.P.; Holm, R.H. A Binuclear Manganese System with Three Isolated Oxidation States: Synthesis, Structures, and Properties of Molecules with a $Mn_2(OR)_2$ Bridge Unit Containing $Mn^{III}Mn^{II}$, and $Mn^{II}Mn^{II}$. *Inorg. Chem.* **1991**, *30*, 4067–4074. [CrossRef]
13. Yu, S.B.; Lippard, S.J.; Shweky, I.; Bino, A. Dinuclear manganese(II) complexes with water and carboxylate bridges. *Inorg. Chem.* **1992**, *31*, 3502–3504. [CrossRef]

14. Gultneh, Y.; Farooq, A.; Liu, S.; Karlin, K.D.; Zubieta, J. Synthesis, structure, and characterization of a phenolate-bridged dimanganese(II) complex of a dinucleating phenol ligand. *Inorg. Chem.* **1992**, *31*, 3607–3611. [CrossRef]
15. Glowiak, T.; Kozlowski, H.; Erre, L.S.; Micera, G. Molecular structure and spectral properties of mono- and dinuclear complexes formed by manganese(II), 2,6-dimethoxybenzoate and 2,2′-bipyridine or 2-methylpyrazine. *Inorg. Chim. Acta* **1995**, *236*, 149–154. [CrossRef]
16. Baldwin, M.J.; Pecoraro, V.L. Energetics of Proton-Coupled Electron Transfer in High-Valent Mn2(μ-O)2Systems: Models for Water Oxidation by the Oxygen-Evolving Complex of Photosystem II. *J. Am. Chem. Soc.* **1996**, *118*, 11325–11326. [CrossRef]
17. Beuken, E.K.V.D.; Feringa, B.L. Bimetallic catalysis by late transition metal complexes. *Tetrahedron* **1998**, *54*, 12985–13011. [CrossRef]
18. Barone, V.; Bencini, A.; Gatteschi, D.; Totti, F. DFT Description of the Magnetic Properties and Electron Localization in Dinuclear Di-μ-oxo-Bridged Manganese Complexes. *Chem. Eur. J.* **2002**, *8*, 5019–5027. [CrossRef]
19. Thompson, L. Polynuclear coordination complexes—From dinuclear to nonanuclear and beyond. *Co-ord. Chem. Rev.* **2002**, 193–206. [CrossRef]
20. Okazawa, A.; Ishida, T.; Nogami, T. Dinuclear Manganese(II) Complex Containing Tetrakis(2-pyridyl)methane as a Spiro-fused Bridge. *Chem. Lett.* **2004**, *33*, 1478–1479. [CrossRef]
21. Ren, Y.; Li, J.; Zhang, F.; Zhang, J.; Guo, H. Crystal Structure and Characterization of a New Mixed-valence Manganese(III/IV) Complex: $[Mn_2(cyclen)_2(\mu\text{-}O)_2](ClO_4)_3 \bullet 4H_2O$. *Chin. J. Chem.* **2005**, *23*, 418–420. [CrossRef]
22. Yang, Y.; Xu, L.; Gao, G.; Li, F.; Liu, X.; Guo, W. An Unexpected Ferromagnetic Coupling in a Dinuclear Manganese(II) Linked Trivacant Heteropolymolybdate Derivative. *Eur. J. Inorg. Chem.* **2009**, *2009*, 1460–1463. [CrossRef]
23. Pantazis, D.A.; Krewald, V.; Orio, M.; Neese, F. Theoretical magnetochemistry of dinuclear manganese complexes: broken symmetry density functional theory investigation on the influence of bridging motifs on structure and magnetism. *Dalton Trans.* **2010**, *39*, 4959. [CrossRef] [PubMed]
24. Yahsi, Y.; Kara, H. Synthesis, structural analysis and magnetic properties of two novel doubly oxygen bridged binuclear manganese(III) and copper(II) complexes with ONO tridentate ligands. *Inorg. Chim. Acta* **2013**, *397*, 110–116. [CrossRef]
25. Brimm, E.O.; Lynch, M.A.; Sesny, W.J. Preparation and Properties of Manganese Carbonyl. *J. Am. Chem. Soc.* **1954**, *76*, 3831–3835. [CrossRef]
26. Mayer, P.; Hosten, E.; Gerber, T.I.A.; Abrahams, A. Synthesis and Structural Characterization of a Novel Ligand-bridged Dimer of Oxorhenium(V). *Bull. Korean Chem. Soc.* **2009**, *30*, 1204–1206.
27. Shopov, D.Y.; Sharninghausen, L.S.; Sinha, S.B.; Borowski, J.E.; Mercado, B.Q.; Brudvig, G.W.; Crabtree, R.H. Synthesis of pyridine-alkoxide ligands for formation of polynuclear complexes. *New J. Chem.* **2017**, *41*, 6709–6719. [CrossRef]
28. Sharninghausen, L.S.; Sinha, S.B.; Shopov, D.Y.; Mercado, B.Q.; Balcells, D.; Brudvig, G.W.; Crabtree, R.H. Synthesis and Characterization of Iridium(V) Coordination Complexes with an N,O-Donor Organic Ligand. *Angew. Chem. Int. Ed.* **2017**, *56*, 13047–13051. [CrossRef]
29. Sunatsuki, Y.; Kishima, Y.; Kobayashi, T.; Yamaguchi, T.; Suzuki, T.; Kojima, M.; Krzystek, J.; Sundberg, M.R. A single tripodal ligand stabilizing three different oxidation states (II, III, and IV) of manganese. *Chem. Commun.* **2011**, *47*, 9149. [CrossRef]
30. Krzystek, J.; Yeagle, G.J.; Park, J.H.; Britt, R.D.; Meisel, M.W.; Brunel, L.C.; Telser, J. High-Frequency and -Field EPR Spectroscopy of Tris(2,4-pentanedionato)manganese(III): Investigation of Solid-State versus Solution Jahn−Teller Effects. *Inorg. Chem.* **2003**, *42*, 4610–4618. [CrossRef]
31. Cotton, F.A.; Extine, M.; Rice, G.W. Sensitivity of the chromium-chromium quadruple bond in dichromium tetracarboxylates to axial coordination and changes in inductive effects. *Inorg. Chem.* **1978**, *17*, 176–186. [CrossRef]
32. Cotton, F.A.; Millar, M. An Exceedingly Short Metal-Metal Bond in a Bis(o-alkoxyphenyl) Dicarboxylatodichromium Compound. *Inorg. Chem.* **1978**, *17*, 2014–2017. [CrossRef]
33. Brown, I.D. Recent Developments in the Methods and Applications of the Bond Valence Model. *Chem. Rev.* **2009**, *109*, 6858–6919. [CrossRef]

34. Brown, I.D.; Altermatt, D. Bond-valence parameters obtained from a systematic analysis of the Inorganic Crystal Structure Database. *Acta Cryst. Sect. B Struct. Sci.* **1985**, *41*, 244–247. [CrossRef]
35. Thorp, H.H. Bond valence sum analysis of metal-ligand bond lengths in metalloenzymes and model complexes. *Inorg. Chem.* **1992**, *31*, 1585–1588. [CrossRef]
36. Liu, W.; Thorp, H.H. Bond valence sum analysis of metal-ligand bond lengths in metalloenzymes and model complexes. 2. Refined distances and other enzymes. *Inorg. Chem.* **1993**, *32*, 4102–4105. [CrossRef]
37. Manohar, A.; Ramalingam, K.; Karpagavel, K.; Bocelli, G. Crystallographic Distances Based Bond Valence Sum (BVS) Analysis on Nickel(II) Complexes Containing Ni-S and Ni-P Bonds. *Adv. Mater. Res.* **2012**, *584*, 84–87. [CrossRef]
38. Kambe, K. On the Paramagnetic Susceptibilities of Some Polynuclear Complex Salts. *J. Phys. Soc. Jpn.* **1950**, *5*, 48–51. [CrossRef]
39. Cotton, F.A.; Murillo, C.A.; Walton, R.A. *Multiple Bonds between Metal Atoms*, 3rd ed.; Springer: Berlin, Germany, 2005.
40. Kahn, O. *Molecular Magnetism*; VCH Publishers Inc.: New York, NY, USA, 1993.
41. Carlin, R.L. *Magnetochemistry*; Springer: Berlin, Germany, 1986.
42. Bruker. *APEX3, SAINT and SADABS*; Bruker AXS Inc.: Madison, WI, USA, 2016.
43. Sheldrick, G.M. *SHELXT*—Integrated space-group and crystal-structure determination. *Acta Cryst.* **2015**, *A71*, 3–8. [CrossRef]
44. Sheldrick, G.M. Crystal structure refinement with *SHELXL*. *Acta Cryst.* **2015**, *C71*, 3–8.